

NOVEL NON-DIRECT CONTACTING MEASUREMENT USING SIGNAL TRANSFER MODEL EXTRACTION AND VERTICAL COUPLING METHOD

Sung-Mao Wu*, Wen-De Chien, and Ren-Fang Hsu

Department of Electrical Engineering, National University of Kaohsiung, No. 700, Kaohsiung University Rd., Nan-Tzu Dist., Kaohsiung, Taiwan, R.O.C.

Abstract—Traditional contacting measurement has numerous disadvantages, including high cost, high damage rate, low mobility, etc. In this study, to resolve these serious problems, a simple, broadband non-contacting loop has been designed to transmit and receive a signal. An equivalent dual-port non-contacting measurement model and a method of vertical coupling capacitance and inductance have been proposed. From the results of the dual-port model simulation and the fabricated sample measurement, a method of signal reconstruction and novel non-contacting measurement is presented.

1. INTRODUCTION

Rapid technological developments in recent decades have led consumers to seek products with high-speed functionality, attractive designs, and increasingly smaller sizes. To achieve more functions using integrated circuits (ICs), the ICs must have many transistors per unit area. Accordingly, measurement devices need to be smaller while remaining precise. Table 1 [1–9] presents several types of probes or probe pins that measure different forms of DUT (device under test) in various ways. Each probe or probe pin has specific advantages. For example, the spring probe pin reduces the pressure when the probe touches the DUT [7, 8], thereby reducing the chance of damaging the DUT. The loop-type probe is the focus of this study.

Measuring the high-density interconnect in ICs using large contacting probes poses significant issues. The most widespread devices for contacting measurement are the VNA (vector network

Received 17 April 2012, Accepted 18 September 2013, Scheduled 24 September 2013


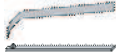



* Corresponding author: Sung-Mao Wu (kokoyou98@gmail.com).

analyzer), ATE (automatic test equipment), and probe station. Despite being so commonly used, these contacting measurement probes have many disadvantages.

First, as mentioned above, the IC is too small for measurements to be done using a contacting probe or SMA connector; shrinking the probe or SMA presents difficulties. The second issue is that when done without sufficient care, contacting measurement usually damages the costly probes or DUTs, leading to significant expense over time. Third, because contacting probes have low mobility, calibration and measurement can take a long time. Every time one moves the contacting probe to a new measurement position, it should leave the surface of the DUT, which adds to the cost. For these reasons, the present research focus on a non-contacting measurement method that is low-cost and easily fabricated. The area of the non-contacting loop, L by L , is only 1.8 mm*1.8 mm and the size can be reduced by a precise process, making the loop small enough to measure tiny DUTs. When the DUT or the measurement position changes, the non-contacting probe can rapidly be moved horizontally. With this high mobility, the non-contacting probe can measure efficiently, thereby reducing the cost.

As indicated in Table 1, the non-contacting loop-type probe has low cost, high mobility, and low likelihood of damaging the DUT or

Table 1. Six package designs for investigating electrical effects.

Performance Probe type	Cost	Mobility	Probability of damaging the DUT	Probability of damaging the probe
	 Air coplanar probe	High	Medium	Medium
 Cantilevered probe	High	Medium	High	High
 Spring contact probe	High	High	Low	Low
 SMA connector	Low	Low	High	High
 Non-contacting Loop-type probe	Low	High	Extreme Low	Extreme Low

the probe, and therefore easily resolves the problems of contacting measurement. In the present research, a quarter of the wavelength and a $50\ \Omega$ micro-strip line was used as the DUT. A coplanar waveguide (CPW) probe was designed as a non-contacting measurement probe and determined the characteristics of the DUT by way of coupling and radiation. The present research contains a dual-port model of non-contacting measurement and a method for signal reconstruction. The measurement and simulation chart shows that the model and coupling method are highly similar. These findings not only can resolve the problems of contact measurement but also can be applied to establish an EMI/EMC model because they feature coupling by a loop-type probe.

2. NON-CONTACTING LOOP DESIGN

For multi-port measurements, the most important considerations are impedance matching and operating bandwidth. How to satisfy these two conditions simultaneously is always a design challenge. When these conditions are met, maximum power transfer can be easily achieved. Designing a loop-type probe with these features is an issue for non-contacting measurement. Past research has provided many different feed-line structures for probes [10–19]. The jagged loop [10], the coplanar waveguide (CPW) loop [11], and the micro-strip line loop [12] address the need for a broadband loop, while the split-ring resonator [13] enhances the coupling. All of these different loop types aim to create a high-coupling probe. Drawing upon this previous work, we have designed a non-contacting probe for non-contacting measurement.

In this paper, the goal is to reconstruct the signal from loop to DUT. If the relation about the signal transfer can be obtained, the non-contact signal transfer will be completed. In order to fulfill this objective, the loop can receive much radiation is designed in this study, a concept of impedance matching is applied for probe designing in this paper [20]. As shown in Fig. 1, when the non-contacting probe is above the DUT, its input impedance can be calculated by the transmission line method. First, the return loss (S_{11}) can be obtained by the actual measurement data. Let $S_{11} = a + jb$, where a is the real part of S_{11} and b is the imaginary part.

$$S_{11} = \frac{Z_{in1} - Z_0}{Z_{in1} + Z_0} = a + jb \quad (1)$$

Then, find the input impedance Z_{in1} :

$$Z_{in1} = \frac{Z_0(1 + S_{11})}{1 - S_{11}} = \frac{Z_0(1 + a + jb)}{1 - (a + jb)} = R_{in1} + jX_{in1} \quad (2)$$

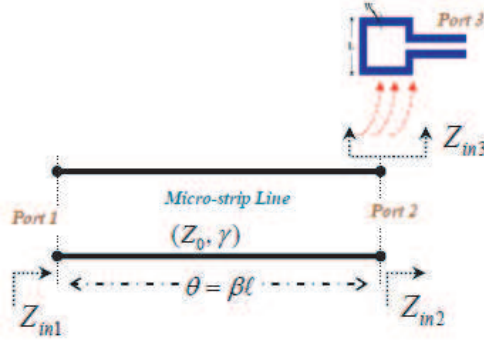


Figure 1. The circuit diagram used to calculate formula (1) [20].

From Equations (1) and (2), find R_{in1} and R_{in1} and X_{in1} :

$$R_{in1} = \frac{50(1 - a^2 - b^2)}{(1 - a)^2 + b^2} \quad (3)$$

$$X_{in1} = \frac{100b}{(1 - a)^2 + b^2} \quad (4)$$

Suppose that the finite transmission line is lossless or has very low loss. Using the input impedance method for a finite transmission line with a load and the equations for R_{in1} and X_{in1} , we can obtain the input impedance at port 1 ($Z_{in1} = R_{in1} + jX_{in1}$):

$$\begin{aligned} Z_{in1} &= Z_0 \frac{Z_L + jZ_0 \tan \beta l}{Z_0 + jZ_L \tan \beta l} = R_{in1} + jX_{in1} \\ &= Z_0 \frac{(Z_{in2} // Z_{in3}) + jZ_0 \tan \beta l}{Z_0 + j(Z_{in2} // Z_{in3}) \tan \beta l} \end{aligned} \quad (5)$$

In formula (5), Z_L in the transmission line will become Z_{in3} , radiation impedance for the loop, and Z_{in2} , a terminal 50Ω at the end of transmission line, in parallel. Z_{in3} and Z_{in2} have their own real and imaginary parts, $Z_{in2} = R_{in2} + jX_{in2}$ and $Z_{in3} = R_{in3} + jX_{in3}$. After calculation, the formula for probe impedance (6) can easily be obtained. A in formula (6)–(8) is $\tan \beta l$ and B is $Z_0 R_{in2}$

$$Z_{in3} = \frac{-Z_0 Z_{in1} Z_{in2} + jZ_{in2} Z_0^2 A}{Z_0 Z_{in1} - Z_0 Z_{in2} + jA(Z_{in1} Z_{in2} - Z_0^2)} \quad (6)$$

$$R_{in3} = B \frac{-Z_0 |Z_{in1}|^2 + Z_0 R_{in1} R_{in2} (1 + A^2 Z_0) - AZ_0^2 (2X_{in1} - AZ_0)}{(Z_0 R_{in1} - Z_0 R_{in2} - AX_{in1} R_{in2})^2 + (Z_0 X_{in1} + AR_{in1} R_{in2} - AZ_0^2)^2} \quad (7)$$

$$X_{in3} = B \frac{AR_{in2} |Z_{in1}|^2 + Z_0 R_{in2} [X_{in1}(1 - A^2) - AZ_0]}{(Z_0 R_{in1} - Z_0 R_{in2} - AX_{in1} R_{in2})^2 + (Z_0 X_{in1} + AR_{in1} R_{in2} - AZ_0^2)^2} \quad (8)$$

Using this impedance formula for the non-contacting loop, one can design a high-coupling, non-contacting loop by impedance matching method. One of the conditions for multi-port measurement, impedance matching, can therefore also easily be satisfied.

Another condition for multi-port measurement, bandwidth, would be satisfied by the CPW structure. In this research, the square loop has a CPW structure as its feed-line. In Fig. 2, the square loop's area, L by L , is $1.8\text{ mm} * 1.8\text{ mm}$ and its width is 0.2 mm . The width of the feed-line is 0.3 mm . The widths of the side grounds of the CPW are not identical. The medium of the loop is PP glue ($\epsilon_\gamma = 4.3$, thickness = 0.15 mm). There are many advantages to having a CPW as the feed-line of a probe [21–24]. First, reducing the volume is a problem, but with the CPW structure the probe can be fabricated easily and have less volume [21]. Second, the feed-line and its ground are close enough that there is low radiation loss when the signal transmits to the loop [22]. Third, different DUTs result indifferent probe impedances, raising difficulties for analysis; there are fewer effects on the impedance of a CPW feed-line when the medium or the dielectric constant is different [23], and potentially less error when the DUT or the medium between the loop and feed-line is different. The most important advantages of the CPW for probe design are ultra-wide bandwidth and good impedance matching [24].

In this study, the probe is designed using HFSS (High Frequency Structure Simulator) electromagnetic simulation software. Simulating a high-efficiency loop with a CPW as its feed-line, the high-efficiency probe can reduce error when analyzing the relationship between loop and DUT, or when comparing the data from the model and from measurement of anFR4 four-layer substrate.

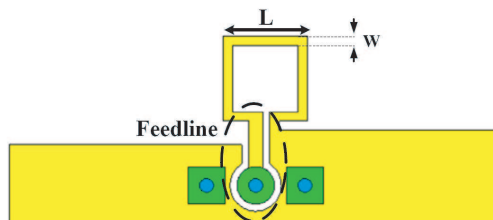


Figure 2. Top view of CPWnon-contacting loop.

3. MEASUREMENT OF THE FR4 FOUR-LAYER SUBSTRATE

The coupling between the probe and the DUT can change when the distance is altered or the probe vibrates. Preventing these situations is an issue for non-contacting measurement. In this study, the most important challenge is measuring the DUT (a micro-strip line) while maintaining a fixed distance between the loop and the DUT. With an FR4 four-layer substrate, the distance between the loop and the DUT can be fixed and vibration can be prevented. After measuring the FR4 four-layer substrate using a probe station, we discuss the relationship and calculate the coupling capacitance and inductance. We design a dual-port non-contacting measurement model based on a single-port non-contacting measurement model, and measure using a probe station.

3.1. The Laminate FR4 Four-layer Substrate

The characteristics of a micro-strip line are determined by the structure of its laminate four-layer substrate. Fig. 3 shows the structure of the substrate in this study. As shown in Table 2, the first layer is the probe's ground and has 0.043 mm thickness. However, there is only a via pad at layer one because the probe and its ground are on the same side, at the second layer, which is 0.035 mm thick. The DUT (micro-strip line, width is 0.2 mm, and length is 20 mm) is at layer three, 0.7 mm from the probe, and the medium is FR4. The fourth layer of the structure is the ground of the DUT, and it is connected

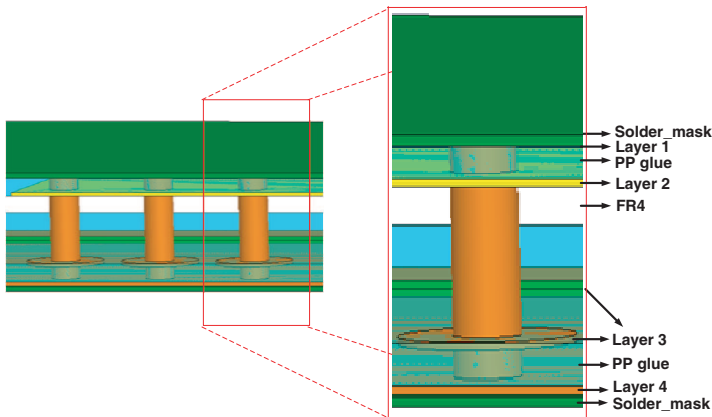


Figure 3. Layer maps of FR4 four-layer substrate.

Table 2. Material and thickness of FR4 four-layer substrate.

Copper (μm)	Layer1	Pad	43	Material (mm)	Soldermask	0.053
	Layer2	Loop	35		PP glue (Polyimide)	0.15
	Layer3	DUT	35		FR4	0.7
	Layer4	GND	43		Soldermask	0.01

to the third layer by the via. In this study, the measurement is at layer four. We contact the via pad by probes and transmit the signal through the via to the loop. In this structure, the main coupling issue is between layers two and three.

3.2. Single-port Measurement

In this research, the objective is that the loop can measure the DUT by extracting the modeling parameter, loop and coupling effect. To reach this goal, the single-port measurement model is completed and dual-port measurement model is extracted to validate the feasibility of this modeling. From Fig. 4, the single-port measurement setup is shown. The DUT, as microstrip line, is placed on the third layer and its ground plane is at the bottom layer, and the measurement loop is placed on the second layer. The first layer is the measurement region by the CASCADE coplanar probe. The signal transmits in line at layer

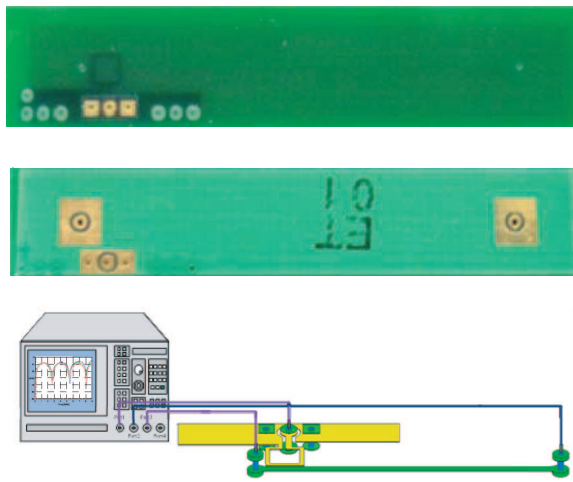


Figure 4. Single-port measurement of the FR4 four-layer substrate.

three and radiates some energy to the dielectric material. Then, the non-contacting loop can receive the radiation energy and be detected by the coplanar probe or the VNA. The measurement data, such as touchstone file (.SnP) can be exported to circuit simulator and designer can use these data to extract model. By the modeling from loop and coupling, the measurement model will initially complete.

3.3. Dual-port Measurement

When the single-port measurement is completed, the dual-port measurement is used to verify the model. The main structure for dual-port non-contacting measurement in this study is presented in Fig. 5 and the measurement setup is the same as single-port measurement. On each side of the DUT are two loop-type probes, which transmit or receive the signal by coupling between the loops and the DUT. Although there are contacting probes on each side of the DUT, the main function of the two contacting probes is to provide the 50Ω load. The capacitance and inductance can be analyzed using this non-contacting measurement structure. The most important step is formulating a method of coupling between the probe and the DUT.

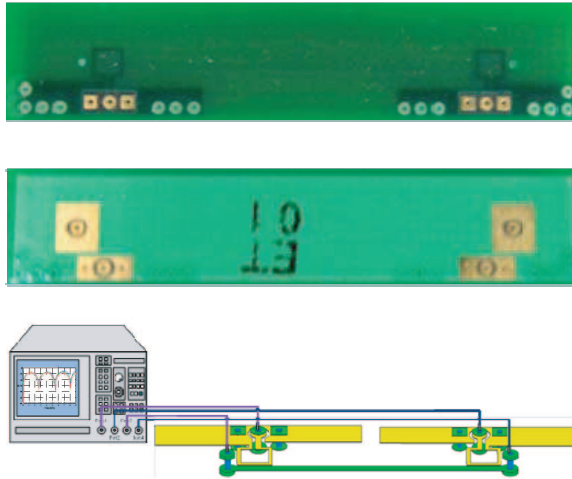


Figure 5. Dual-port measurement of FR4 four-layer substrate.

4. THE COUPLING METHOD AND PROBE MODEL

In this study, the most important issues are how to achieve coupling between the probe and the DUT and how to enhance the model's

reliability. If we calculate the probe's parameters and the coupling parameters between the probe and the DUT, these two issues will be resolved. Four parameters for the method were determined: the coupling capacitance and inductance, and the other two parameters of the loop, determined by the method. This coupling method not only can restore the signal but also can be applied to establish an EMI/EMC model.

4.1. Calculating the Probe's Parameters

The probe parameters are its resistance-inductance and capacitance-inductance with GND. According to formula (9) [25, 26] and Fig. 6(a), the cross-section area A times the resistivity ρ and divided by the total length of the probe L yields the probe's resistance, which in this case is 0.015Ω . Capacitive coupling with GND is obtained using formula (10) [26] and Fig. 6(b), in which area A is divided by the distance d between the ground and the feed-line. The value of the probe capacitance in this study is 0.045 pF . Although obtaining these two values is not the purpose of this research, doing so can greatly enhance the reliability of the model by reducing the number of unknown values.

$$R = \rho \frac{L}{A1} \quad (\Omega) \quad (9)$$

$$C = \varepsilon_\gamma \varepsilon_0 \frac{A2}{d} \quad (\text{Farad}) \quad (10)$$

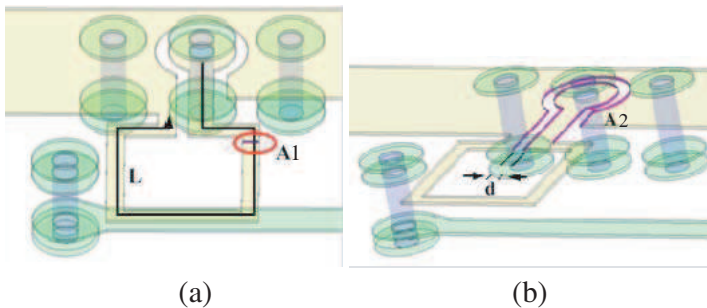


Figure 6. Probe resistance and capacitance calculated with (a) formula (9) and (b) formula (10).

4.2. Calculating the Coupling Parameters

The key issue in this study is the relationship between the loop and the DUT. The loop is like an antenna, and the coupling method between

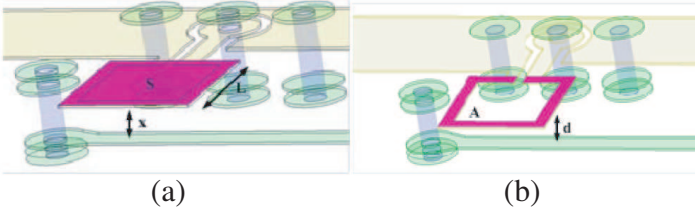


Figure 7. Calculating the coupling and distinguishing the field using (a) formulas (11) and (12), and (b) formula (10).

the loop and the DUT should be determined to formulate a coupling method. In other words, whether the antenna should be measured on a near-field or far-field range needs to be established. According formula (11) [27], where x is distance for distinguishing the far-field or near-field, L represents loop length 1.8 mm and λ is wavelength corresponding to operating frequency, and Fig. 7, the frequency from 0 to 32 GHz is a near-field measurement under a fixed distance of 0.7 mm and a loop length of 1.8 mm in the FR4 substrate. For the bandwidth of the model in this research, the frequency from 0 to 9 GHz based on Z_{in3} is entirely far-field measurement, so the relationship between the probe and the DUT must be analyzed using a far-field coupling formula.

Because the main coupling method of the loop-type probe is magnetic field coupling, the most relevant equations are from Faraday's law and the Biot-Savart law, expressed in formulas (12) and (13), where μ_0 is permeability $4\pi \times 10^{-7}$ for this case, I represents the transmitted current in the loop, L shows the loop length, and x is the distance with the same as formula (11). These two formulas show that the distance between loop and DUT, and the loop length, might yield different values for the magnetic field intensity. As Fig. 7 and formula (13) show, the loop length L and the distance between probe and DUT x give the coupling inductance, which in the present study is 1.2816 nH. With formula (14) and Fig. 7, the coupling area A is taken from the parallel edge areas, and the distance d is the distance between loop and DUT. The value of the coupling capacitance is 0.0696 pF.

$$x = \frac{2L^2}{\lambda} \quad (11)$$

$$\oint_c E \cdot dl = - \int_s - \frac{dB}{dt} \cdot ds + \oint_c (v \times B) \cdot dl \quad (12)$$

$$B = \frac{\mu_0 I L^2}{\mu \cdot 2\pi \left(x^2 + L^2/4\right) \left(\sqrt{x^2 + L^2/2}\right)} \text{(Weber/cm}^2\text{)} \quad (13)$$

$$L = NBS/I \text{(Henry)} \quad (14)$$

With the four important parameters in the Table 3 extracted in this study, the performance between the loop and the DUT, as microstrip line, can be known by the modeling using the lump component. The magnitude of radiation loss can be obtained. By acquiring the loss from radiation, the received signal of loop can subtract it or make some mathematical transformation to obtain the signal at DUT. In other words, the loop signal can be reconstructed to the DUT. Furthermore, the non-contact measurement can be completed.

Table 3. Four parameters calculated by the method.

R_a	C_g	C_m	L_m
0.015 Ω	0.045 pF	0.0696 pF	1.2816 nH

5. ESTABLISHING THE MODEL AND COMPARING WITH MEASUREMENT AND SIMULATION

It is important to establish a dual-port non-contacting measurement model. With a highly reliable model and a method of signal loss between probe and DUT, this novel non-contacting measurement can be substituted for contacting measurement. Thus far we have calculated the coupling inductance and capacitance. The next step is to establish a non-contacting measurement model with the four values calculated in this study.

5.1. Establishing the Model

As indicated above, four parameters have been obtained in this model, two of which are the coupling capacitance and coupling inductance between probe and DUT. Although these are not all the parameters, the two coupling parameters can assist with the method for signal restoration. In addition, the unknown numbers in the model can be reduced, thereby enhancing the model's reliability.

First of all, the four parameters obtained in this study should be fixed to optimize the other unknown numbers of the single-port model. After that, the dual-port model can be designed with those values.

5.2. Single-port Radiation Model

Figure 8 and Table 4 show the single-port model in this study. The CPW loop has resistance R_a , self-inductance L_a , capacitance C_g between ground and loop and mutual inductance L_g coupling between its ground plane and signal line. The coupling capacitance and inductance between probe and DUT are C_m and L_m . L_d is the inductance of the via extracted from formula (15) [28]; discontinuance of the inductance when the probe is above the DUT changes the impedance. Because the GND of the probe is large, the DUT may couple with the GND of the probe. When the signal transmits to the end of the micro-strip line, the large GND of the probe is above the micro-strip line. This micro-strip line with GND both above and below is like a strip-line. C_{lg} is the coupling capacitance between the DUT and the probe's GND. The extracted value is shown in the formula (10).

$$L = 5.08h \left[\ln \left(\frac{4h}{D} \right) + 1 \right] \quad (15)$$

Figure 9 compares the FR4 four-layer substrate measurement, single-port radiation model, and simulation. In this study, the loop is designed and simulated under a real environment using HFSS software. Fig. 9 shows the return loss $S(2, 2)$ of the line and insertion loss $S(1, 2)$ between the loop and terminal of line at the far-end, and the coupling parameter $S(1, 3)$ between loop at port 3 and terminal of line at the

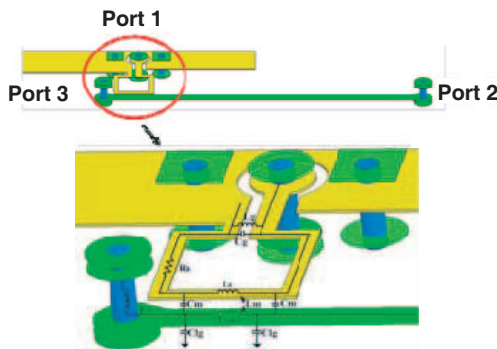


Figure 8. The single-port radiation model.

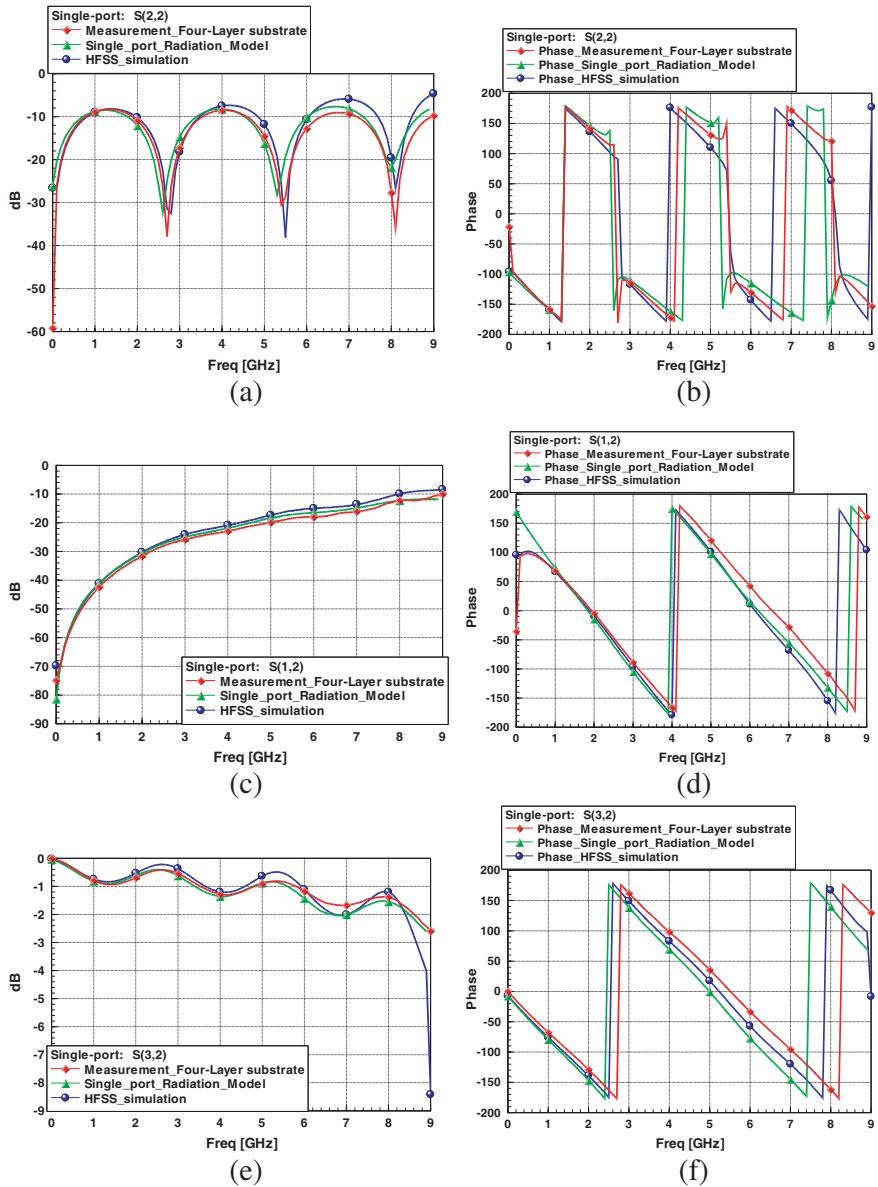
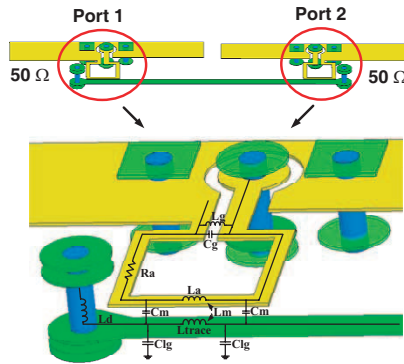


Figure 9. Radiation model compared with measurement and simulation. (a) $S_{(2,2)}$ dB, (b) $S_{(2,2)}$ phase, (c) $S_{(1,2)}$ dB, (d) $S_{(1,2)}$ phase, (e) $S_{(1,3)}$ dB, (f) $S_{(1,3)}$ phase

Table 4. Parameters of the radiation model.

Inductance	L_a	L_g
	1.7593 nH	3.1069 nH
	L_d	L_m
	0.8084 nH	1.2816 nH
Capacitance	C_{lg}	C_g
	0.15 pF	0.045 pF
	C_m	
Resistance	R_a	
	0.015 Ω	

**Figure 10.** The dual-port non-contacting measurement model.

near-end relative to loop. Using the highly reliable single-port model, we can design a highly reliable dual-port model.

5.3. Dual-port Non-contacting Measurement Model

In this study, the main purpose is to design a novel dual-port non-contacting measurement. When the single-port model was established, the problem became how to make it into a dual-port model. In Fig. 10, a dual-port model is designed based on two single-port models side by side above the DUT. When the single-port models are on both sides of the DUT, both sides will have discontinuous L_d and coupling between the DUT and the probes' GND. If the single-port model is reliable enough for the loop-type probe, the dual-port model should also be reliable enough for the FR4 four-layer substrate non-contacting measurement in this study.

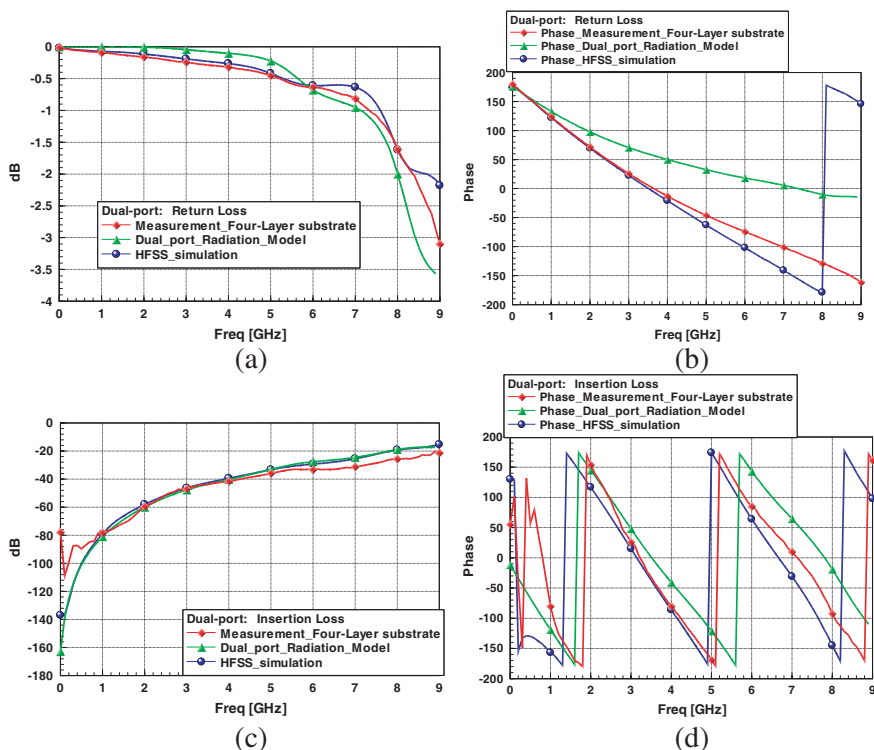


Figure 11. Insertion loss and return loss of non-contacting model. (a) $S_{(1,1)}$ dB, (b) $S_{(1,1)}$ phase, (c) $S_{(2,1)}$ dB, (d) $S_{(2,1)}$ phase

Figure 11 presents the data for dual-port non-contacting measurement, comparing the FR4 four-layer substrate, the non-contacting measurement model, and the HFSS simulation. Both insertion loss and return loss are shown. As the graphs indicate, the non-contacting measurement model is highly similar to the four-layer substrate measurement. Only the phase of return loss and insertion loss are a little mismatch, because the much radiation energy can dissipate at higher frequency. The loss energy can lead to change the equivalent length between the loop and DUT, and generate the serious mismatch for the multi-reflection. When the similarity is high enough, probe contacting measurement can be substituted by the model in this study.

6. CONCLUSION

This research has proposed a method of vertical coupling capacitance and inductance between a non-contact loop and a DUT, as well as a dual-port non-contacting measurement model designed using

a single-port model. With the low cost, high mobility, and other advantages of loop-type probes, non-contacting measurement can resolve the problems presently encountered with contacting measurement. Comparison of the fabricated sample, dual-port non-contacting measurement model, and HFSS simulation shows that the model and the coupling method for non-contacting measurement can substitute for contacting measurement. In addition, the coupling method and modeling can be used to develop an EMI/EMC measurement model.

REFERENCES

1. Smith, K., P. Hanaway, M. Jolley, R. Gleason, E. Strid, T. Daenen, L. Dupas, B. Knuts, E. J. Marinissen, and M. Van Dievel, "Evaluation of TSV and micro-bump probing for wide I/O testing," *2011 IEEE International Test Conference (ITC)*, 1–10, Sep. 20–22, 2011.
2. Soejima, K., M. Kimura, Y. Shimada, and S. Aoyama, "New probe microstructure for full-wafer, contact-probe cards," *1999 Proceedings: 49th Electronic Components and Technology Conference*, 1175–1180, 1999.
3. Huang, J.-T., K.-Y. Lee, C.-S. Wu, C.-Y. Lin, and S.-H. Shih, "Using micro-electroforming and micro-assembly technology to fabricate vertical probe card," *International Conference on Electronic Materials and Packaging, 2006. EMAP 2006*, 1–5, Dec. 11–14, 2006.
4. Tsao, Y.-C., J.-J. Tang, and Y.-L. Hsieh, "Analysis of probing effects on solder bump," *Proceedings of 6th Electronics Packaging Technology Conference, 2004. EPTC 2004*, 303–307, Dec. 8–10, 2004.
5. Kumar, S., S. Rao, T. K. Guan, and F. Harun, "Influence of wafer probing against initial bonding," *2010 34th IEEE/CPMT International Electronic Manufacturing Technology Symposium (IEMT)*, 1–8, Nov. 30, 2010–Dec. 2, 2010.
6. Kim, J. Y., H. J. Lee, H. J. Choi, S. J. Lee, and S. W. Moon, "Design, fabrication and mechanical characterization of vertical micro contact probe," *5th IEEE Conference on Sensors, 2006*, 1155–1158, Oct. 22–25, 2006.
7. Zapatka, M. and R. Ziser, "An introduction to coaxial RF probing solutions for mass-production tests," *74th ARFTG Microwave Measurement Symposium, 2009*, 1–6, Nov. 30, 2009–Dec. 4, 2009.
8. Andes, J. and E. Bogatin, "The socket response to current packaging and test trends," *IEEE/CPMT/SEMI 29th International*

- Electronics Manufacturing Technology Symposium, 2004*, 97–99, Jul. 14–16, 2004.
9. Hung, S.-K., C.-F. Tsai, Y.-P. Hsu, D.-J. Tzou, M.-H. Lin, and L.-C. Fu, “Automatic probe alignment for atomic force microscope,” *IEEE International Conference on Mechatronics, 2005. ICM’05*, 909–912, Jul. 10–12, 2005.
 10. Lin, S.-Y., S.-K. Yen, W.-S. Chen, and P.-H. Cheng, “Printed magnetic field probe with enhanced performances,” *Asia Pacific Microwave Conference, 2009. APMC 2009*, 649–652, Dec. 7–10, 2009.
 11. Kim, J.-M., W.-T. Kim, and J.-G. Yook, “Resonance-suppressed magnetic field probe for EM field-mapping system,” *IEEE Transactions on Microwave Theory and Techniques*, Vol. 53, No. 9, 2693–2699, Sept. 2005.
 12. Funato, H. and T. Suga, “Magnetic near-field probe for GHz band and spatial resolution improvement technique,” *17th International Zurich Symposium on Electromagnetic Compatibility, 2006. EMC-Zurich 2006*, 284–287, Feb. 27, 2006–Mar. 3, 2006.
 13. Ren, Z., M. S. Boybay, and O. M. Ramahi, “Near-field probes for subsurface detection using split-ring resonators,” *IEEE Transactions on Microwave Theory and Techniques*, Vol. 59, No. 2, 488–495, Feb. 2011.
 14. Boybay, M. S. and O. M. Ramahi, “Experimental and numerical study of sensitivity improvement in near-field probes using single-negative media,” *IEEE Transactions on Microwave Theory and Techniques*, Vol. 57, No. 12, 3427–3433, Dec. 2009.
 15. Masuda, N., N. Tamaki, T. Kuriyama, J. C. Bu, M. Yamaguchi, and K. Arai, “High frequency magnetic near field measurement on LSI chip using planar multi-layer shielded loop coil,” *2003 IEEE International Symposium on Electromagnetic Compatibility*, Vol. 1, 80–85, Aug. 18–22, 2003.
 16. Sujintanarat, P., P. Dangkhom, S. Chaichana, K. Aunchaleevarapan, and P. Teekaput, “Analysis of electromagnetic emission from PCB by using a near-field probe,” *International Symposium on Communications and Information Technologies, 2006. ISCIT’06*, 208–211, Oct. 18, 2006–Sept. 20, 2006.
 17. Ren, Z., M. S. Boybay, and O. M. Ramahi, “Near-field subsurface detection in lossy media using single split resonator probe,” *IEEE MTT-S International Microwave Workshop on Wireless Sensing, Local Positioning, and RFID, 2009. IMWS 2009*, 1–3, Sept. 24–25, 2009.

18. Shi, J., R. E. DuBroff, K. Slattery, M. Yamaguchi, and K.-I. Aral, "A study of the probe induced disturbances on the near-field measurement," *2003 IEEE International Symposium on Electromagnetic Compatibility, 2003. EMC'03*, Vol. 1, 127–130, May 16, 2003.
19. Boyer, A., S. Bendhia, and E. Sicard, "Characterisation of electromagnetic susceptibility of integrated circuits using near-field scan," *Electronics Letters*, Vol. 43, No. 1, 15–16, Jan. 4, 2007.
20. Huang, C.-H. R.-F. Hsu, S.-M. Wu, Y.-C. Tang, and C.-C. Chen, "Radiation modeling and performance reconstructing of signal connection in package substrate using non-contacting probe," *Asia-Pacific Microwave Conference Proceedings (APMC), 2011*, 1035–1038, Dec. 5–8, 2011.
21. Al-Nuaimi, M. K. T., "Compact CPW-fed antenna loaded with dumbbell slot defected ground structure," *Loughborough Antennas and Propagation Conference (LAPC), 2011*, 1–4, Nov. 14–15, 2011.
22. Saladi, A. S. R., J. R. Panda, and R. S. Kshetrimayum, "An E-shaped CPW-fed folded-slot antenna for the 2.45 GHz RFID applications," *2011 International Conference on Communications and Signal Processing (ICCSP)*, 363–366, Feb. 10–12, 2011.
23. Jung, D., C.-H. Ahn, and K. Chang, "Ultra wideband CPW fed modified ring antenna," *IEEE Antennas and Propagation Society International Symposium, 2009. APSURSI'09*, 1–4, Jun. 1–5, 2009.
24. Hettak, K., G. Y. Delisle, G. A. Morin, S. Toutain, and M. Stubbs, "A novel variant 60-GHz CPW-fed patch antenna for broadband short range wireless communications," *IEEE Antennas and Propagation Society International Symposium, 2008. AP-S 2008*, 1–4, Jul. 5–11, 2008.
25. Kalhor, H. A., "Comparison of Ampere's circuital law (ACL) and the law of Biot-Savart (LBS)," *IEEE Transactions on Education*, Vol. 31, No. 3, 236–238, Aug. 1988.
26. Cheng, D. K., *Field and Wave Electromagnetics*, 2nd edition, Addison-Wesley, 1989.
27. Balanis, C. A., *Antenna Theory: Analysis and Design*, Wiley, Hoboken, NJ, 2005.
28. Howard Johnson and Martin Graham, *High Speed Digital Design: A Handbook of Black Magic*, Prentice Hall, 1993.